Conformational Dynamics and the Energetics of Protein−Ligand Interactions: Role of Interdomain Loop in Human Cytochrome P450 Reductase†

Alex Grunau,‡ Kalotina Geraki,§ J. Günter Grossmann,§ and Aldo Gutierrez*,‡

Department of Biochemistry, University of Leicester, The Henry Wellcome Building, Lancaster Road, Leicester LE1 9HN, U.K., and Molecular Biophysics Group, Science and Technology Facilities Council Daresbury Laboratory, Daresbury Science and Innovation Campus, Warrington, Cheshire, WA4 4AD, U.K.

Received March 28, 2007; Revised Manuscript Received May 15, 2007

ABSTRACT: A combination of mutagenesis, calorimetry, kinetics, and small-angle X-ray scattering (SAXS) has been used to study the mechanism of ligand binding energy propagation through human cytochrome P450 reductase (CPR). Remarkably, the energetics of 2′,5′-ADP binding to R597 at the FAD-binding domain are affected by mutations taking place at an interdomain loop located 60 Å away. Either deletion of a 7 amino acid long segment (T236-G237-E238-E239-S240-S241-I242) or its replacement by poly-proline repeats (5 and 10 residues) results in a significant increase in 2′,5′-ADP enthalpy of binding (ΔH_B). This is accompanied by a decrease in the number of thermodynamic microstates available for the ligand−CPR complex. Moreover, the estimated heat capacity change (ΔC_p) for this interaction changes from −220 cal mol^{-1} K^{-1} in the wild-type enzyme to −580 cal mol^{-1} K^{-1} in the deletion mutant. Pre-steady-state kinetics measurements reveal a 50-fold decrease in the microscopic rate for interdomain (FAD → FMN) electron transfer in the deletion mutant ($k_{obs} = 0.4$ s^{-1}). Multiple turnover cytochome *c* reduction assays indicate that these mutations impair the ability of the FMN-binding domain to shuttle electrons from the FAD-binding domain to the cytochrome partner. Binding of 2′,5′-ADP to wild-type CPR triggers a large-scale structural rearrangement resulting in the complex having a more compact domain organization, and the maximum molecular dimension (D_{max}) decreases from 110 Å in ligand-free enzyme to 100 Å in the ligand-bound CPR. The SAXS experiments also demonstrate that what is affected by the mutations is indeed the relative diffusional motion of the domains. Furthemore, *ab initio* shape reconstruction and homology modeling would suggest that—in the deletion mutant—hindering of domain motion occurs concomitantly with dimerization. The results presented here show that the energetics of this highly localized interaction (2′,5′-ADP binding) have a global character, and are highly sensitive to functional structural dynamics involving distal domains. These findings support early theoretical studies which postulate a single protein molecule to be a real, independent thermodynamic ensemble.

One of the main challenges faced by protein sciences nowadays is to build a coherent view of binding energy propagation to remote sites within a macromolecule, and its effect on functional dynamics. This is of paramount importance in understanding the mechanisms behind the vast array of cell signaling events mediated by proteins. Central to this challenge is the need for this phenomenon to be formulated within the framework of thermodynamics, enabling these long-range effects to be understood in terms of universal molecular driving forces.

Cytochrome P450 reductase (CPR[1]) is a structurally complex multidomain protein (Figure 1) (*1*). It contains two flavin-binding domains as redox centers (FAD- and FMN-binding domains). An additional linker domain, with no catalytic function, is present between the two redox domains. Domain motion in CPR is directly related to the electrochemical events required for its physiological function. Two electrons—in the form of a hydride ion (H^-)—are donated to CPR by NADPH (an obligatory two-electron donor) through the FAD-binding domain, and are subsequently transferred one by one to a cytochrome P450 partner (an obligatory one-electron acceptor) *via* a different domain, the FMN-binding domain. Stepwise one-electron transfer is achieved by disproportionation of the electron pair through interdomain electron transfer (FAD → FMN) (*2*). This electron-transfer step is kinetically gated by the diffusional motion required for the two domains to sample favorable conformations (*3*). Previous temperature-jump and pre-steady-state (*3*, *4*) kinetics studies have shown that binding of 2′,5′-ADP, the NADPH coenzyme's binding moiety, triggers conformational dynamics that propagate through the

† This work was funded by the Wellcome Trust. A. Gutierrez is a Wellcome Trust Career Development Research Fellow (069246).

* Corresponding author. E-mail: afg2@le.ac.uk. Tel: (+44) 0116 229 7085. Fax: (+44) 0116 229 7085.

‡ University of Leicester.

§ Science and Technology Facilities Council Daresbury Laboratory.

[1] Abbreviations: CPR, cytochrome P450 reductase; 2′,5′-ADP, adenosine 2′,5′-diphosphate; BES, *N*,*N*-bis(2-hydroxyethyl)-2-aminoethanesulfonic acid; ITC, isothermal titration calorimetry; DSC, differential scanning calorimetry; SAXS, small-angle X-ray scattering; D_{max}, maximum linear dimension; R_g, radius of gyration; I_o, forward scattering intensity; FMN, flavin mononucleotide; FAD, flavin adenine dinucleotide; BM_3-P450, cytochrome P450 (CYP102), isolated from *Bacillus megaterium*; NOS, nitric-oxide synthase.

10.1021/bi700596s CCC: $37.00
Published on Web 06/20/2007

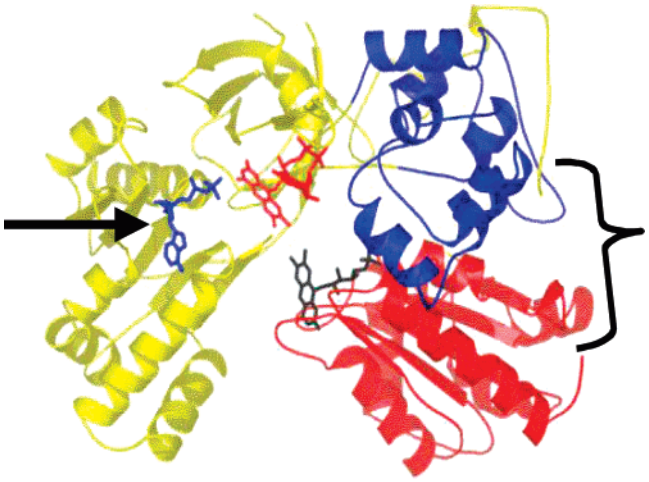

FIGURE 1: Crystal structure of coenzyme-bound rat CPR in its oxidized form. The different structural domains are indicated: FAD-binding domain (yellow), linker "hinge" domain (blue), and FMN-binding domain (red) (*1*). The two flavin cofactors, FAD (red) and FMN (black), are separated by only 4 Å in this structure. However the experimentally measured interdomain electron-transfer rate is 9 orders of magnitude *lower* than the intrinsic rate predicted from this conformation, suggesting that CPR adopts a more elongated shape in solution (*3*). An arrow (←) indicates the $NADP^+$ coenzyme (blue) bound to R597 in the FAD-binding domain. The location corresponding to the unstructured segment (T236-G237-E238-E239-S240-S241-I242) of the interdomain loop where the mutations take place is indicated by brackets. These residues could not be solved in the crystal structure. The distance between R597 and this segment is approximatly 60 Å.

macromolecule resulting in catalytically important domain movements. These features make this enzyme an ideal model in which to study the mechanisms of (ligand) binding energy propagation and its effects on functional dynamics.

In the CPR enzyme the FMN-binding domain is linked to the other two domains through a loop 14 amino acids long (residues 231 to 244) (Figure 1). This loop does not seem to make any contact with the rest of the protein. These features are required in order for the FMN-binding domain to shuttle electrons from the FAD-binding domain to cytochrome P450 partners. Furthermore, 7 amino acids lying at the center of this loop (T236-G237-E238-E239-S240-S241-I242) could not be seen in the crystal structure, implying flexibility or multiple conformations (Figure 1). The residues located up- and downstream of this segment, A235 and R243, respectively, are 62 and 54 Å away from the actual site where binding of 2′,5′-ADP takes place (R597). In the studies reported here, a deletion mutant was constructed which lacks this 7 amino acid long peptide. Additionally we carried out poly-glycine and poly-proline substitutions (5 and 10 amino acids) at this unstructured segment of the interdomain loop. The rationale behind these mutations is to modify the diffusional motion of the domains, while leaving the interaction between 2′,5′-ADP and R597 completely unaffected. This experimental design aims to probe any distal contribution of domain motion to the energetics of ligand binding.

EXPERIMENTAL PROCEDURES

Materials. NADPH, 2′,5′-ADP, and horse heart cytochrome *c* were purchased from SIGMA. All other chemicals were of analytical grade.

Site-Directed Mutagenesis and Protein Purification. Mutants were produced using the QuickChange site-directed mutagenesis kit (Stratagene, La Jolla, CA). To facilitate annealing of the mutagenic primers, 5G and 5P mutants were obtained first and then used as templates for the 10G and 10P mutants, respectively. In all cases, the entire CPR gene was sequenced to ensure that no spurious changes had occurred during mutagenic PCR reactions. Amino acid sequencing was carried at the Protein Nucleic Acid Chemistry Laboratory (PNACL) at the University of Leicester using the Amersham Pharmacia Biotech T7 sequencing kit and protocols (GE Healthcare, USA). Wild-type human fibroblast CPR (lacking the N-terminal membrane-anchoring region) and mutants were expressed in *Escherichia coli* BL21(DE3)pLysS from appropriate pET15b plasmid constructs.

Proteins were purified according to a procedure described recently (*4*). Binding stoichiometry (as assessed by isothermal titration calorimetry) was used as a quality control to ascertain no adenosine nucleotide contaminants remain bound to the protein at the end of the purification procedures. Only protein preparations displaying a binding stoichiometry (n) of 1 ± 0.1 were deemed to be suitable for these studies. Protein concentration was calculated using a molar extinction coefficient of $\epsilon_{450nm} = 22000\ M^{-1}\ cm^{-1}$.

Isothermal Titration Calorimetry (ITC). Protein samples for microcalorimetry experiments were prepared daily from 50% glycerol stocks kept at −20 °C. ITC experiments were conducted using a VP-ITC microcalorimeter (Microcal Inc., MA). Data acquisition and analysis were carried out using ORIGIN 7.0 (Microcal Inc., MA). Ligand binding to wild-type CPR (or mutants) was quantified by fitting the evolved heat per injection to the Wiseman equation (*5*). Fitting of the binding isotherm was carried out through multiple iterations until a minimum χ^2 value was obtained. Reported values are the average of at least two runs. In order for the Wiseman equation to yield reliable values, the unitless parameter c should be between 10 and 1000. This parameter is defined as $c = M_{total} \times K_{B,}$ where M_{total} is the total binding site concentration and K_B is the equilibrium binding constant (*5*). The protein concentration used in the cell (M_{total}) was chosen so as to give c values in the 100−300 range (typically 5−10 μM). As described in our previous calorimetry studies with the same ligand (*4*), control titrations were also done at 1 μM ($c = 20$) and 3 μM ($c = 60$) (protein concentration) to verify that the measured values were concentration independent. In the case of the deletion mutant, additional data analysis assuming a putative dimer conformation (i.e., using a molar extinction coefficient of $\epsilon_{450nm} = 44000\ M^{-1}\ cm^{-1}$) give identical ΔH_B values for 2′,5′-ADP binding, and a binding stoichiometry $n = 2$ (per dimer). A detailed discussion of ITC data analysis has been published elsewhere (*5*). Heat capacity change (ΔC_p) values were calculated from temperature-dependence plots of ΔH_B values. In order to obtain ΔC_p values as accurate as experimentally possible, isothermal titrations were carried out at temperature intervals of 2.5 °C from 5 °C to 35 °C.

Differential scanning calorimetry (DSC) experiments were carried out at the BBSRC/EPSRC Biological Microcalorimetry Facility at the University of Glasgow according to protocols published elsewhere (*6*). The rate of heating was 60 °C/h. Thermal melting of wild-type CPR and mutants

was found to be irreversible at pH 7.0 (see Supporting Information). BES [*N*,*N*-bis(2-hydroxyethyl)-2-aminoethanesulfonic acid] 100 mM, pH 7.0, was the buffer used for these and the rest of the experimental studies described in this paper. The rationale behind this choice of buffer has been published previously (*4*).

Pre-Steady-State and Multiple Turnover Kinetic Measurements. Single turnover kinetic measurements for the reductive half-reaction in wild-type CPR and mutants were carried out using a Bio-sequential SX.18MV stopped-flow spectrophotometer (Applied Photophysics Ltd), and according to protocols previously developed by the authors (*2*, *3*).

Steady-state kinetic assays with NADPH as electron donor and cytochrome *c* as electron acceptor were performed at 25 °C ,and the initial velocity of the reaction was measured by reduction of cytochrome c^{3+} at 550 nm ($\Delta\epsilon_{550nm} = 21.1$ mM^{-1} cm^{-1}) using a Cary-300 UV/visible spectrophotometer. Reaction mixtures contained 7 nM (0.5 μg/1 mL assay) CPR, 50 μM NADPH and variable concentrations of cytochrome *c* (1−200 μM). Data was fitted to the Michaelis−Menten equation using Origin 7.0 (MicroCal Inc., MA).

Solution X-ray Scattering Data Collection and Analysis. SAXS measurements were carried out at station 2.1 of the Synchrotron Radiation Source, Daresbury, U.K., using a position-sensitive multiwire proportional counter. Scattering profiles were collected at two different sample-to-detector distances, 1 m and 4.25 m, covering a momentum transfer range of 0.01 $Å^{-1} < s < 0.5$ $Å^{-1}$ with $s = 4\pi \sin \Theta / \lambda$ (where 2Θ is the scattering angle and λ the X-ray wavelength of 1.54 Å). Samples were measured at a temperature of 25 °C and at concentrations of 15 μM (1 mg/mL), 45 μM (3 mg/mL), 75 μM (5 mg/mL), and 300 μM (20 mg/mL) and exposed to X-rays between 5 and 30 min in 1 min time frames. The measurement procedure (including concentration series) safeguarded against effects such as radiation damage and interparticle interference, which were negligibly small. In order to determine the effect of 2′,5′-ADP binding in the experimental scattering profile, this ligand was added in stoichiometric amounts (15 μM to 200 μM). The low dissociation constant of this ligand under these experimental conditions ensures saturation ($K_d = 53$ nM; 100 mM BES, pH 7.0; 25 °C) (*4*).

The data was analyzed with the ATSAS 2.1 software package (*42*), and procedures followed closely those described previously (*7*). The radius of gyration (R_g), the intraparticle distance distribution function $p(r)$, and the forward scattering intensity (I_o) were calculated from the experimental scattering data using the indirect Fourier transform method with the program GNOM (*8*). Model-independent molecular shapes were calculated using GASBOR (*9*). This *ab initio* procedure represents the protein as an assembly of spheres corresponding to the number of amino acid residues and uses simulated annealing to find the optimal 3D arrangement in agreement with the experimental scattering data. Up to 15 independent GASBOR runs were averaged using DAMAVER (*10*) and SUPCOMB (*11*) to obtain a typical molecular shape. In the case of the deletion mutant, GASBOR calculations were done using a 2-fold symmetry (assuming a dimer). Shape reconstructions included constraints in order to approximate an overall conformation as the one observed in the NOS reductase dimer (PDB code: 1TLL) (*12*). An initial molecular model of the CPR dimer was built based on NOS reductase and subsequently optimized with BUNCH (*36*) using the experimental scattering data of the ligand-bound deletion mutant. The BUNCH algorithm allows the building of multidomain models using the information from high-resolution structures, adds missing peptide segments, and refines them against scattering data (*36*). Scattering profile simulations from crystal coordinates were carried out using CRYSOL (*13*).

Analytical Gel Filtration. A HPLC Precision Column PC 3.2/20 (Amersham Pharmacia Biotech) was operated using an Agilent 1100 instrument (flow rate, 0.1 mL/min; operational pressure, 1.5 MPa, 25 °C) (Agilent Technologies, U.K.). The column's gel volume is 2.4 mL, the injected volume was 10−50 μL, and the concentration of loaded sample was ∼60 μM [4 mg/mL]. Column calibration was carried out using a set of molecular weight markers (MW-GF-200, SIGMA), which includes two proteins of molecular weight similar to that of the wild-type CPR and (dimeric) deletion mutant (albumin, 66 kDa; alcohol dehydrogenase, 150 kDa).

RESULTS

The Energetics of 2′,5′-ADP Binding Are Sensitive to Mutations at the Distal Interdomain Loop. Previous calorimetry studies with human CPR demonstrated the bipartite nature of NADP(H) in binding to this enzyme, the adenosine moiety (2′,5′-ADP) providing the primary element in coenzyme binding (*4*). Binding isotherms for the interaction of 2′,5′-ADP with wild-type CPR and mutants are shown in Figure 2A (25 °C). Remarkably, in the poly-proline (5P, 10P) and deletion mutants the actual heat evolved during the binding of 2′,5′-ADP to R597 at the distal FAD-binding domain differs unambiguously from the observed ΔH_B in the wild-type enzyme. This difference is biggest in the case of the deletion mutant and amounts to a 70% increase at 35 °C (−33 kcal mol^{-1}) compared with the wild-type enzyme (−20 kcal mol^{-1}) (Figure 2B). This pattern is especially evident in the poly-proline mutants (5P, 10P), showing a more negative enthalpic change even at the lowest temperature examined in this study (5 °C). At low temperature ΔH_B values for the wild-type and deletion mutant converge at around −13 kcal mol^{-1}.

In a protein−ligand interaction, the entropy term ($T\Delta S_B$) indicates the change in the number of microstates through which the ligand-bound protein macrostate is realized from the free state. As is the case of ΔH_B values, the entropy changes for this highly localized interaction are nevertheless distinctive in the interdomain mutants as compared to the wild-type CPR enzyme (Figure 2C, Table 1). The entropy change ($T\Delta S_B$) values observed for 2′,5′-ADP binding to the poly-proline and deletion mutants are more negative than those observed for binding of the same ligand to the wild-type enzyme. This indicates that the number of available thermodynamic microstates (multiplicity) has significantly diminished in these mutants (Figure 2C). The difference in $T\Delta S_B$ between the poly-glycine and poly-proline mutants is likely to reflect the relative differences in chain stiffness introduced by these mutations. There is a correlation between these $T\Delta S_B$ values and the characteristic ratio (an indicator of chain stiffness) of each isolated polypeptide (5G, 10G, 5P, and 10P) (Figure 3B).

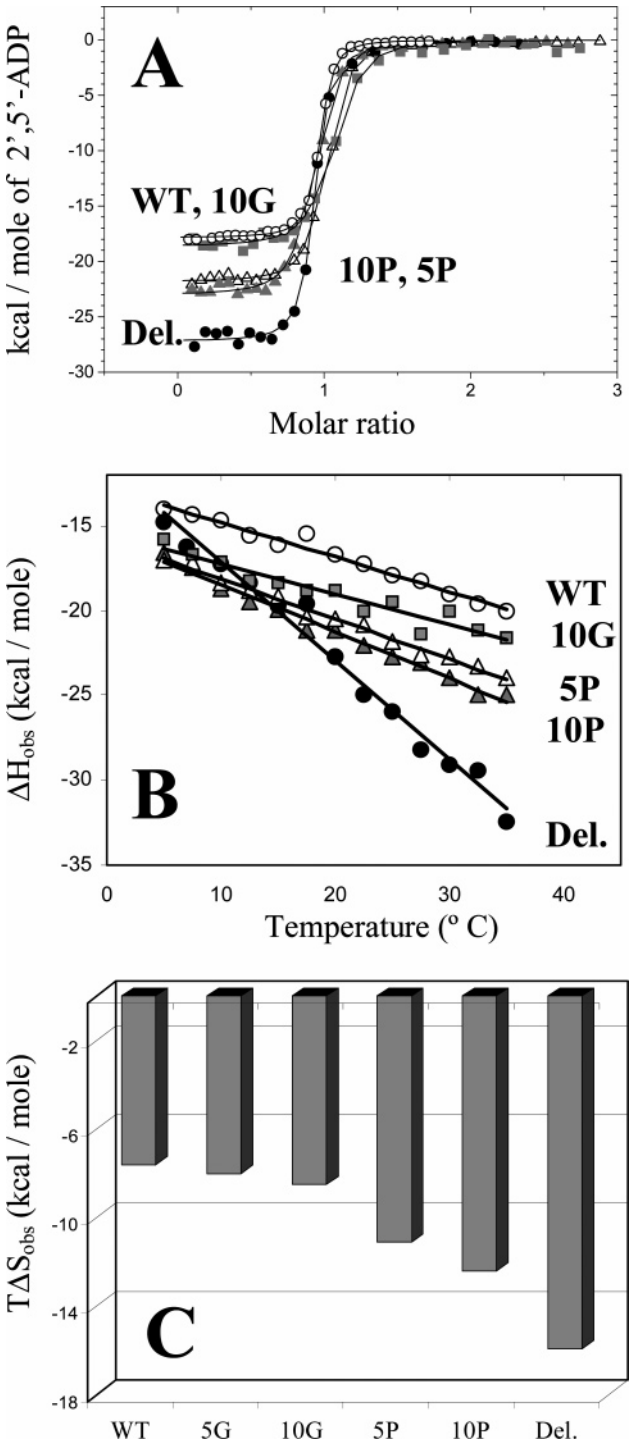

FIGURE 2: Thermodynamics of 2′,5′-ADP binding to wild-type CPR and interdomain loop mutants. Panel A: Binding isotherms (25 °C) for the titration of 2′,5′-ADP into wild-type CPR (black open circles), 10G mutant (gray closed squares), 5P mutant (open black triangles), 10P mutant (gray closed triangles), and deletion mutant (black closed circles). The experimental points are fit to the Wiseman equation (black lines) (*5*). Molar ratio is that of a monomer unit (deletion mutant). For clarity, the binding isotherm for the 5G mutant is not shown. Panel B: Temperature dependence (5 °C to 35 °C) of the observed enthalpy (ΔH_{obs}) for the binding of 2′,5′-ADP. Wild-type CPR (black open circles), 10G mutant (gray closed squares), 5P mutant (open black triangles), 10P mutant (gray closed triangles), and deletion mutant (black closed circles). Lines represent the linear least-squares regression to the experimental data (Table 1). For clarity, the data for the 5G mutant is not shown. Panel C: Estimated entropy of binding ($T\Delta S_B$) at 25 °C of wild-type CPR, 5G, 10G, 5P, 10P, and deletion mutants.

Table 1: Thermodynamic Parameters for the Binding Interaction of CPR and Mutants with 2′,5′-ADP[a]

protein	ΔC_p (cal mol^{-1} K^{-1})	ΔG_B (kcal mol^{-1})	ΔH_B (kcal mol^{-1})	$T\Delta S_B$ (kcal mol^{-1})	$K_{B,obs} \times 10^6$ (M^{-1}) (25 °C)
wild-type	−220 (0.99)	−9.8	−18	−7.6	19 ± 0.3
5G	−180 (0.90)	−10	−18	−8.0	15 ± 2.0
10G	−180 (0.92)	−10	−19	−8.5	17 ± 0.6
5P	−240 (0.99)	−9.9	−22	−11	20 ± 1.4
10P	−280 (0.98)	−9.9	−23	−12	18 ± 1.3
deletion	−580 (0.98)	−10	−26	−16	32 ± 2.4
FAD domain[b]	−300 (0.97)	−10	−19	−9.2	28 ± 2.2

[a] Buffer conditions: 100 mM, pH 7.0. Temperature: 25 °C. [b] Data for the FAD-binding domain taken from Grunau, A., et al. (2006), ref 4.

Modification of the distal interdomain loop also results in differences in estimated heat capacity changes (ΔC_p) for the 2′,5′-ADP−R597 interaction (Table 1). The magnitude of the changes in ΔC_p of the mutants mirrors the order observed in Figure 2C with the deletion mutant ($\Delta C_p = -580$ cal mol^{-1} K^{-1}, $R^2 = 0.98$), showing a remarkable approximately 3-fold decrease in relation to the wild-type ($\Delta C_p = -210$ cal mol^{-1} K^{-1}, $R^2 = 0.99$). Differential scanning calorimetry (DSC) measurements carried out at the same experimental conditions as ITC (100 mM BES pH 7; 5−10 μM protein concentration) indicate that onset of thermal unfolding in wild-type CPR and in the mutants takes place at temperatures higher than 40 °C. The melting temperature (T_m) for wild-type, 10P, and deletion mutants was 52 °C, 51 °C, and 47 °C, respectively (under these conditions unfolding was irreversible; scan rate, 60 °C/h) (see Supporting Information). As shown in Figure 2B the experimental temperature interval for ITC measurements in this study is from 5 °C to 35 °C. Therefore differences in thermal stability are highly unlikely to contribute to the differences in the calculated ΔC_p for 2′,5′-ADP binding.

Despite the striking differences in ΔH_{obs} and ΔS_B values of the mutants and the wild-type, ΔG_B values for the interaction of 2′,5′-ADP with R597 remain unchanged in the temperature range used in these studies (5 °C−35 °C), indicating no change in the thermodynamic stability of the ligand−protein complex (Figure 3A) (Table 1). The observed equilibrium binding constant ($K_{B,obs}$) for the binding of 2′,5′-ADP to wild-type CPR is 19 × 10^6 M^{-1} ($c = 190$, 25 °C). In the mutant series, this value ranges from 15 × 10^6 M^{-1} (5G mutant, $c = 150$) to 32 × 10^6 M^{-1} (deletion mutant, $c = 160$) (Table 1). Thus, binding of 2′,5′-ADP to wild-type and the mutants is fundamentally an isoergonic process, with not significant differences in Gibbs free energy change. This result fully validates our experimental design (i.e., the primordial interaction is not affected by any of the mutations). Furthermore, it indicates that the energetics changes observed in the mutants have a nonlocal origin.

Kinetic Effects of Mutations at the Interdomain Loop. Under single-turnover conditions, stoichiometric reduction by NADPH results in interdomain electron transfer (FAD → FMN) with the concomitant formation of the one-electron reduced FMN blue-semiquinone (FMN_{sq}, $\lambda = 600$ nm) (*2*−*4*). Our previous studies have shown that this step (i.e., FMN_{sq} formation) is kinetically gated by the diffusional motion required for the domains to sample configurations close enough for electron transfer to occur (*3*). Thus, FMN_{sq}

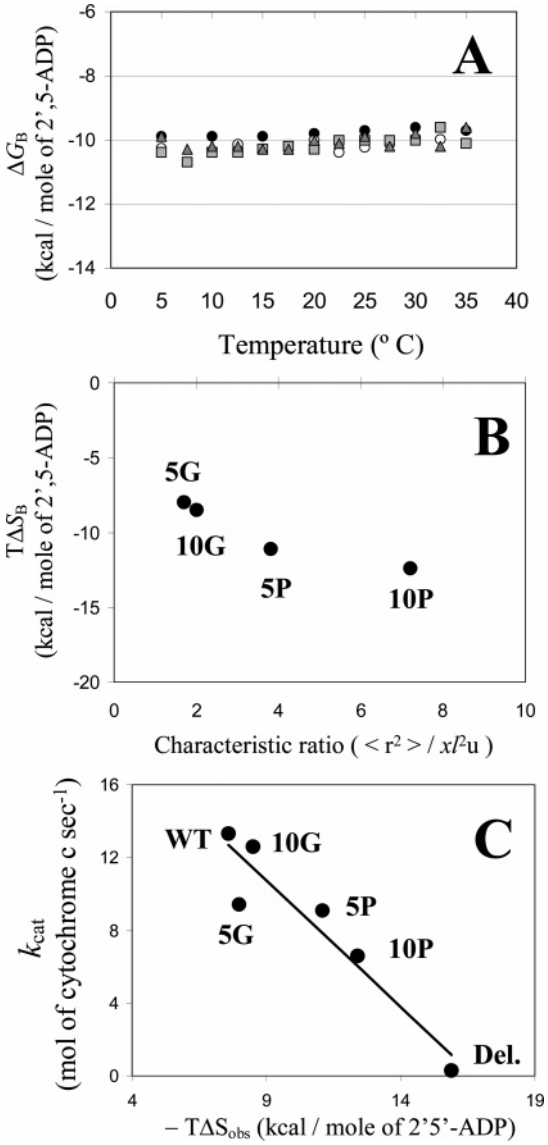

FIGURE 3: Gibbs free energy for 2′,5′-ADP binding. Correlation of entropy changes against conformational and kinetic parameters. Panel A: Estimated change in Gibbs free energy (ΔG_B) for the interaction between CPR and 2′,5′-ADP in the temperature interval 5 °C to 35 °C. Wild-type CPR (black open circles), 10G mutant (gray closed squares), 10P mutant (gray closed triangles), and deletion mutant (black closed circles). For clarity, the data for the 5G and 5P mutants is not shown. Panel B: Plot for 2′,5′-ADP binding entropy changes ($T\Delta S_B$) against the intrinsic chain stiffness (characteristic ratio) of the respective homopeptide (5G, 10G, 5P, and 10P mutants). *Ab initio* characteristic ratio values ($\langle r^2\rangle_o/xl^2u$) for poly-proline and poly-glycine peptides (x = 5 and 10) were taken from Schimmel, P. R., and Flory, P. J. (*25*). r = radius of gyration; x = number of residues; l = end-to-end distance; u = conformational energy. Panel C: Plot of the estimated entropy change ($T\Delta S_B$) for 2′,5′-ADP binding (25 °C) against k_{cat} values for steady-state cytochrome *c* reduction (25 °C). Line represents the linear least-squares regression to the experimental data, R^2 = 0.89.

formation rates actually report on domain diffusion rates (see Figure 1 legend) (*2*−*4*). Kinetic transients from stopped flow spectroscopy measurements of FMN blue-semiquinone formation in wild-type CPR and mutant (at a pseudo-stoichiometric amount of NADPH) are shown in Figure 4A. The observed rate for the deletion mutant is k_{obs} = 0.4 s^{-1} (transient "d"). There is a noticeable initial lag phase in the deletion mutant spanning approximately 100 ms (transient

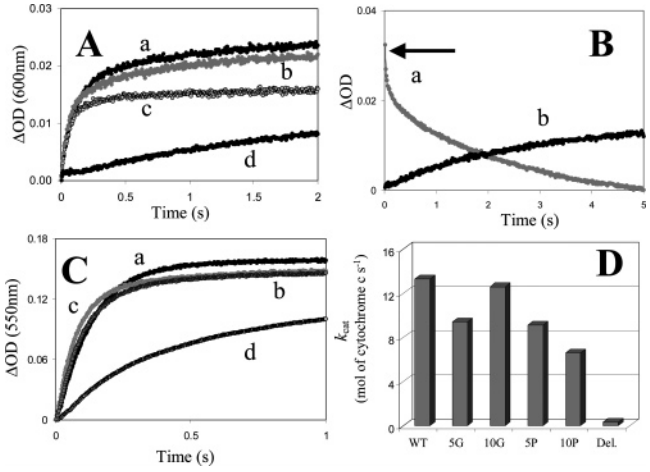

FIGURE 4: Pre-steady-state and multiple turnover kinetics. Panel A: Interdomain electron-transfer kinetics (λ = 600 nm). Stopped-flow rapid mixing spectrophotometry at 25 °C. Wild-type CPR and mutants [10 μM] were reacted against stoichiometric amount of NADPH. The transients report on the formation of the one-electron blue-semiquinone species at the FMN domain (FMN_{sq}) upon initial reduction of the FAD cofactor by NADPH. The observed rates are as follows: wild-type (transient "a"), k_{obs1} = 20 s^{-1}; k_{obs2} = 3 s^{-1}, 10G mutant (transient "b"), k_{obs1} = 20 s^{-1}; k_{obs2} = 1.5 s^{-1}; 10P mutant (transient "c"), k_{obs1} = 16 s^{-1}; k_{obs2} = 1.5 s^{-1}; and deletion mutant (transient "d"), k_{obs} = 0.4 s^{-1}. Panel B: Flavin reduction kinetics in the deletion mutant transient "a" (λ = 450 nm), an arrow (←) indicates the starting point of the amplitude change. Transient "b": Interdomain electron-transfer transient for the deletion mutant (λ = 600 nm). Panel C: Single-turnover reduction of cytochrome *c* by wild-type CPR and mutants (λ = 550 nm, 25 °C). The observed rates are as follows: wild-type (transient "a"), k_{obs} = 15 s^{-1}; 10G mutant (transient "b"), k_{obs} = 15 s^{-1}; 10P mutant (transient "c"), k_{obs1} = 17 s^{-1}; and deletion mutant (transient "d"), k_{obs1} = 3.2 s^{-1}, k_{obs2} = 0.3 s^{-1}. For clarity, kinetic transients for the 5G and 5P mutants are not shown in panels A, B, and C. Panel D: Multiple turnover steady-state cytochrome *c* reduction assay (25 °C).

"d"). Deletion of the 7 amino acid segment thus results in a 50-fold decrease in the observed interdomain electron-transfer rates as compared to the wild-type enzyme (k_{obs} = 20 s^{-1}). Absorption changes at λ = 450 nm report on total flavin reduction rates (i.e., FAD and FMN cofactors) upon hydride transfer from NADPH to FAD. As shown in Figure 4B, flavin reduction in the deletion mutant is strongly biphasic with observed rates k_{obs1} = 15 s^{-1} and k_{obs2} = 0.4 s^{-1}. The observed rate for the initial flavin reduction step (i.e., NADPH → FAD, k_{obs1} = 15 s^{-1}) compares well with the one observed in wild-type CPR, k_{obs1} = 18 s^{-1} (*2*). Therefore initial hydride transfer in the deletion mutant appears to be as fast as in the wild-type mutant. Indeed, superimposition on to the 600 nm transient reveals that approximately 40% of the total amplitude change associated with flavin reduction ($k_{obs1,}$ 450 nm) takes place within the lag phase observed prior to formation of the FMN_{sq} (600 nm) (Figure 4B). Thus, these findings indicate that the low interdomain electron-transfer rate (FAD → FMN) observed in the deletion mutant is not due to a decrease in the initial step of the reductive half-reaction (i.e., FAD reduction).

The decrease in interdomain electron transfer in the deletion mutant in turn leads to low cytochrome *c* reduction rates (k_{obs1} = 3.2 s^{-1}, k_{obs2} = 0.3 s^{-1}). Cytochrome *c* is a redox protein known to be reduced by CPR precisely *via* the semiquinone species in the FMN-binding domain (Figure 4C) (*4*). Under these pre-steady-state conditions, interdomain

(FAD → FMN) and interprotein (FMN → cytochrome *c*) electron-transfer rates remain basically unchanged in the other mutants (Figure 4C). Surprisingly, even the introduction of a 10 poly-proline peptide in the interdomain loop results in *single turnover* rates similar to those of the wild-type CPR (wild-type, $k_{obs} = 15\ s^{-1;}$ 10P mutant, $k_{obs} = 17\ s^{-1}$) (Figure 4C, transients "a" and "c"). However, the effect of the proline mutations is evident when steady-state rates (k_{cat}) are measured (Figure 4D). The turnover number for the 10P mutant ($k_{cat} = 6.6\ s^{-1}$) is roughly half of that of the wild-type enzyme ($k_{cat} = 13\ s^{-1}$). Once again, deletion of the original loop segment (T236-G237-E238-E239-S240-S241-I242) seems to be the most detrimental modification in terms of the kinetic properties of the mutant series (Figure 4D). The calculated turnover number for the deletion mutant ($k_{cat} = 0.3\ s^{-1}$) is fundamentally the same as the observed rate in single-turnover measurements of interdomain electron transfer ($k_{obs} = 0.4\ s^{-1}$) (Figure 4A, transient "d" $k_{obs} = 0.4\ s^{-1}$). This indicates that, in the deletion mutant, the impaired interdomain microscopic step (FAD → FMN) has now become the absolute rate-limiting step for the steady-state reduction of cytochrome *c*.

Taken together, these observations suggest that what is primarily affected by the poly-proline and deletion mutations—in kinetic terms—is the ability of the FMN-binding domain to *repeatedly* undergo motional shuttling between FAD and its cytochrome partner. Interestingly, there is a linear correlation ($R^2 = 0.89$) between turnover numbers for cytochrome *c* reduction, and $T\Delta S_B$ values for 2′,5′-ADP binding (a measure of the multiplicity of microstates available to the protein−ligand complex) (Figure 3C).

Solution X-ray Scattering Studies of Wild-Type CPR and Mutants in the Presence and Absence of 2′,5′-ADP Ligand. As shown in Figure 5A the experimental scattering profiles for the ligand-free 10P and deletion mutants differ markedly from that of the wild-type enzyme. The maximum linear dimension (D_{max}) for the ligand-free wild-type CPR is 110 Å, compared to 94 and 104 Å for the 10P and deletion mutant, respectively (Table 2 and Figure 5A, inset). Similarly, the distribution of scattering mass of each mutant (as indicated by the radius of gyration, R_g), is also different from that of wild-type CPR, with R_g values of 28 and 35 Å for the 10P and deletion mutant, respectively, as opposed to 32 Å for the wild-type enzyme (Table 2). These observations clearly demonstrate the significant effect that these mutations at the interdomain loop have on the overall conformation of the protein.

Remarkably, binding of 2′,5′-ADP to wild-type CPR results in a 10 Å decrease in molecular diameter (D_{max} = 110 and 100 Å for free and bound CPR, respectively) (Figure 5B and inset). This transition from the free CPR to the ligand-bound complex is also accompanied by a decrease in the radius of gyration (R_g) from 32 to 30 Å (Table 2). Therefore 2′,5′-ADP binding does induce a structural change in the wild-type enzyme, altering fundamental conformational features of the macromolecule. This observation agrees with previous relaxation kinetics (temperature-jump) experiments (*3*, *17*). These studies proposed that the observed increase in interdomain electron transfer upon 2′,5′-ADP binding is due to this ligand positioning the domains into a more favorable orientation (*17*). In the 10P mutant (Figure 5C), the magnitude and nature of the changes triggered by ligand binding are similar to those observed in the wild-type (D_{max} = 94 and 82 Å for the free and bound forms, respectively) (Figure 5C, inset) (Table 2). Noticeably, in the deletion mutant, 2′,5′-ADP binding fails to trigger any significant difference in either the estimated size (D_{max} = 104 and 102 Å for free and bound forms, respectively) or the radius of gyration (R_g = 35 Å for both free and bound forms) (Figure 7A) (Table 2).

Ab initio shape reconstructions from the corresponding experimental scattering profiles highlight the difference between the molecular envelopes of ligand-free wild-type CPR and ligand-free 10P mutant (Figure 6, left panels) as well as the domain reorganization caused by 2′,5′-ADP binding in both wild-type CPR and 10P mutant (Figure 6, right panels). Insertion of a 10P repeat in the interdomain loop (Figure 6B) results in a restriction of the spatial volume sampled by the structural domains in solution, as compared to the elongated arrangement adopted by the domains in the wild-type CPR (ligand-free) (Figure 6A). Binding of 2′,5′-ADP to either wild-type CPR or 10P mutant appears to restrict the flexibility of the macromolecule's domains even further (Figure 6, right panels). As a result, the ligand-bound forms, especially the 10P mutant, resemble the $NADP^+$-bound crystal structure of rat CPR (Figure 1 and legend). These observations neatly illustrate the intrinsic dynamic motion of the different domains within this enzyme, as well as the fundamental role played by the interdomain loop in their conformational equilibrium. A detailed study of the conformational dynamics specific to each domain using 1-electron reduced CPR and a combination of SAXS and NMR is now in its final stages (Ellis, J., et al., manuscript in preparation).

Scattering data analysis for the deletion mutant was performed assuming the presence of a dimeric particle in solution. The value for the forward scattering intensity (which is proportional to the molecular mass) of this mutant is twice the value (within errors) obtained for wild-type CPR and 10P mutant (data not shown), suggesting that this mutant is primarily dimeric at the concentration range used for SAXS measurements (15−300 μM). Analytical gel filtration experiments corroborate this conclusion (Figure 7C). Wild-type CPR and the deletion mutant show distinctive retention times, each of them migrating primarily as a single band. The short retention time of the deletion mutant indicates a molecular weight bigger than that of wild-type CPR (see inset in Figure 7C). The estimated molecular weight from these experiments is 160 kDa for the deletion mutant as opposed to ~70 kDa for the wild-type enzyme (the known molecular weight for the wild-type CPR construct used in these studies is 68 kDa as calculated from the primary structure). Intriguingly, the scattering profile for the deletion mutant shows a noticeable shoulder in the intermediate scattering angle region around $s = 0.17\ Å^{-1}$ (Figures 5A and 7) which is present in neither the wild-type nor 10P mutant scattering profile. In the light of the gel filtration results, this feature would indicate a structural architecture with a characteristic length scale of ~40 Å arising from the monomer−monomer association of the deletion mutant. Moreover, the fact that ligand binding has no major effect on the overall structural integrity of this mutant would indicate a rigid structural association consistent with interprotomer interactions (Figure 7A, inset). In order to gain insight into the conformation of the deletion mutant,

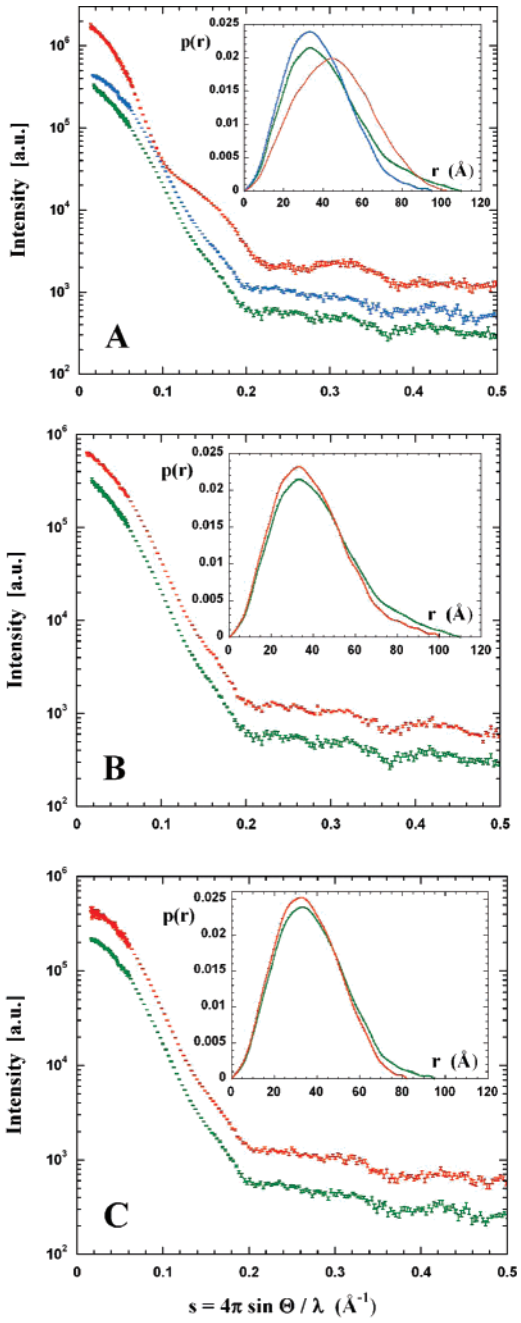

FIGURE 5: SAXS results for solutions of wild-type CPR and mutants. Panel A: Ligand-free species. Experimental scattering profile of ligand-free wild-type CPR (green), 10P mutant (blue), and deletion mutant (red). Errors bars for each scattering profile are shown. Inset: Intraparticle distance distribution function $p(r)$ for ligand-free wild-type CPR (green line), 10P mutant (blue line), and deletion mutant (red line). Panel B: Wild-type CPR. Experimental scattering profile of ligand-free (green) and 2′,5′-ADP-bound (red). For clarity the scattering profile of the 2′,5′-ADP-bound enzyme has been artificially shifted upward by multiplying the intensity values (y-axis) by a factor of 2. Errors bars for each scattering profile are shown. Inset: Intraparticle distance distribution function $p(r)$ for ligand-free (green line) and ligand-bound wild-type CPR (red line). Panel C: 10P mutant. Experimental scattering profile of ligand-free (green line) and 2′,5′-ADP-bound (red line). For clarity the scattering profile of the 2′,5′-ADP-bound mutant has been artificially shifted upward by multiplying the intensity values (y-axis) by a factor of 2. Errors bars for each scattering profile are shown. Inset: Intraparticle distance distribution function $p(r)$ for ligand-free (green line) and ligand-bound 10P mutant (red line). The area under $p(r)$ is scaled to unity in all three insets (panels 5A, 5B, and 5C).

Table 2: Structural Parameters Deduced from Solution X-ray Scattering Profiles[a]

protein	D_{max} (Å)	R_g (Å)
wild-type	110	32.3
wild-type + ligand	100	30.1
10P	94	28.9
10P + ligand	82	27.3
deletion	104	35.0
deletion + ligand	103	34.5

[a] Ligand: 2′,5′-ADP. Sample conditions: 100 mM BES, pH 7.0. Temperature: 25 °C. Error margins for D_{max} and R_g are of the order of 5% and 2%, respectively.

a combination of molecular modeling and scattering profile simulation was carried out based on nitric-oxide synthase (NOS), a member of the CPR-diflavin protein family. Each NOS monomer comprises a CPR module (FAD- and FMN-binding domains) plus a calmodulin-binding linker and an oxygenase module (heme-binding domain) (*12* and references therein). The crystal structure of the fully assembled dimer of the neuronal NOS CPR-module (also called "reductase module") has been reported recently (*12*). A dimeric model of human CPR was built upon this structure (Figures 8A and 8C), and a simulated scattering profile from this CPR dimer was calculated (Figure 7B).

The small-angle region calculated from this NOS-based dimer model produces a side maximum at around $s = 0.17$ Å^{-1}, similar to that observed in the experimental scattering profile of the deletion mutant (Figure 7B). Nevertheless, the high goodness-of-fit value ($\chi = 12.1$) indicates a poor fit and suggests further structural reorganization not accounted for this molecular homology model. Therefore, a model for the deletion mutant dimer was obtained using the BUNCH program (See Experimental Procedures). The BUNCH model reproduces the observed shoulder and other features of the experimental scattering profile more realistically ($\chi = 5.0$) (Figure 7B). An *ab initio* shape reconstruction from the experimental scattering profile of the deletion mutant (free and bound forms) was performed assuming a 2-fold symmetry constraint. The result of this model-independent reconstruction is shown in Figure 8 with the BUNCH model superimposed. Unlike the calculations for wild- type CPR, the experimental scattering data of the deletion mutant produces molecular shapes that are less affected by 2′,5′-ADP binding (see Supporting Information). Our models obtained from the SAXS data do not provide unequivocal information about the orientation of individual domains and their redox cofactors. Nevertheless, the low pre- and steady-state rates observed with the deletion mutant suggest that, despite the close packing brought about by dimeric association, conformational sampling critically required for electron transfer has been severely limited in this mutant. These observations point toward a significant reduction in the structural degrees of freedom of the domains in the ligand-free dimer. This would explain the relatively minor effect that 2′,5′-ADP binding has in the already constrained domains (Figures 7A, 8; Table 2) (see Supporting Information for additional *ab initio* shapes of the deletion mutant).

In the crystal structure of the reductase dimer of neuronal NOS, interaction between the monomers occurs mainly through their respective FMN-binding domains (*12*), the isolated FAD-binding domain being apparently unable to

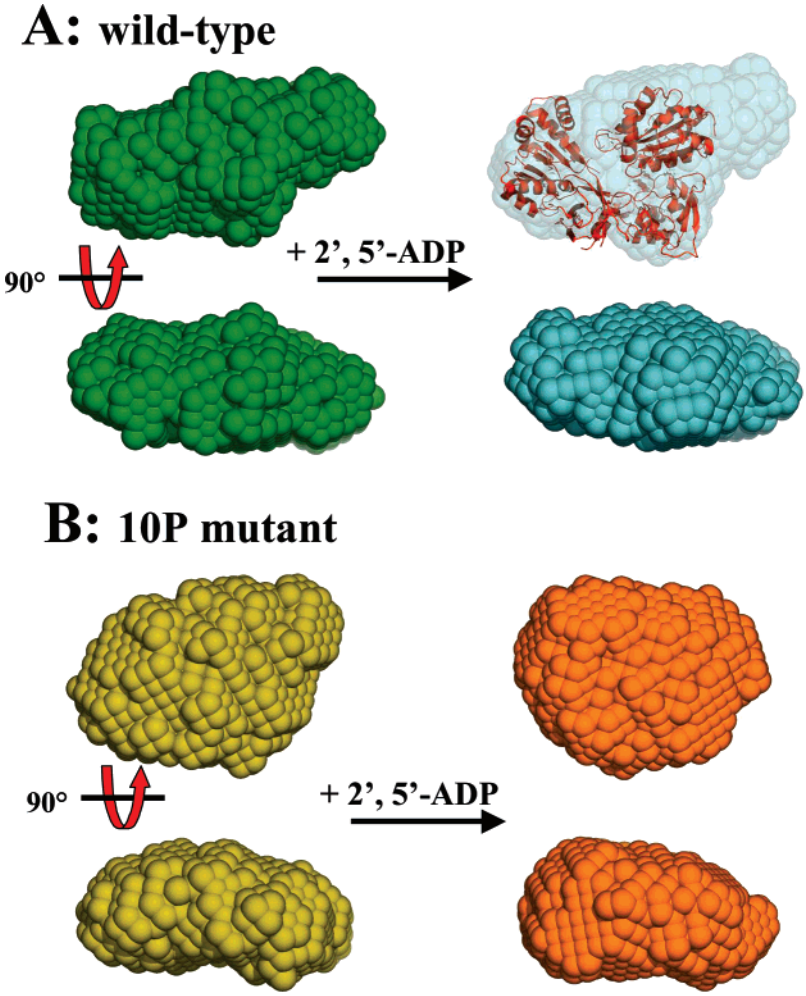

FIGURE 6: *Ab initio* shape representations for wild-type CPR and 10P mutant. The panels on the left display two perpendicular shapes for each of the two proteins in their ligand-free state. The right-hand panel gives the corresponding shapes in the 2′,5′-ADP-bound conformation. Shape reconstructions were done with GASBOR, and a representative average was obtained from 10 models with DAMAVER (*9*, *10*). All shapes have been aligned with respect to the ligand-bound wild-type conformation. The ribbon model of rat CPR crystal structure (Figure 1) has been superimposed for comparison purposes.

form a dimer itself (*14*). The residues involved in these interprotomer salt bridges (E790, K820, D979, and R 979) are not conserved in either the other isoforms (endothelial and inducible NOS) or CPR (see Figure 2 in ref *12*). Recently, a functional dimer of BM3−P450—another CPR-homologue protein—has also been reported (*15*). Thus, CPR-diflavin proteins seem to contain structural motifs that could potentially be recruited into forming interprotomer bonds. Deletion of the T236-G237-E238-E239-S240-S241-I242 loop segment in CPR would therefore bring into play non-native domain interactions that promote dimerization in this mutant. Calorimetry and stopped-flow measurements with CPR were carried out routinely at concentrations in the micromolar range 10 μM (monomer) (see Experimental Procedures), and scattering profiles were collected with sample concentrations from 15 to 300 μM. Interestingly, the turnover number from steady-state kinetics measurements ($k_{cat} = 0.3\ s^{-1}$) is the same as the interdomain electron-transfer rate ($k_{obs} = 0.4\ s^{-1}$) despite a 1000-fold difference in protein concentration used for these experiments (steady-state assay = 7 nM, pre-steady stopped-flow spectrophotometry = 10 μM). As discussed above, these rates are defined by the motional ability of the domains and by their relative orientation. The similarity between these rates would therefore indicate that the structural modifications induced by the deletion mutation—underpinning its kinetic properties—are manifested uniformly within a broad concentration range (7 nM to 300 μM).

DISCUSSION

Biological electron transfer underpins essential processes such as respiration and photosynthesis. These reactions are carried out by redox cofactors contained in single proteins or independent domains which are generally arranged along the thermodynamic driving force (e.g., proton motive force, $\Delta\mu H^+$; equilibrium potential differential between redox centers, ΔE). As a consequence, large-scale conformational dynamics are a fundamental aspect of these reactions (*16* and references therein). Furthermore, biological electron-transfer reactions do not appear to be optimized for speed but rather are kinetically gated (often in the millisecond time scale) by constrained diffusive motions needed to bring redox centers within quantum tunneling distances (*16*). Our previous relaxation kinetics (*3*, *17*) and calorimetry (*4*) studies established that 2′,5′-ADP binding energy triggers domain reorganization affecting electron-transfer rates as well as recognition of a cytochrome partner protein. Therefore, in this paper, we have attempted to study the relation between the energetics of ligand binding and the functional dynamics

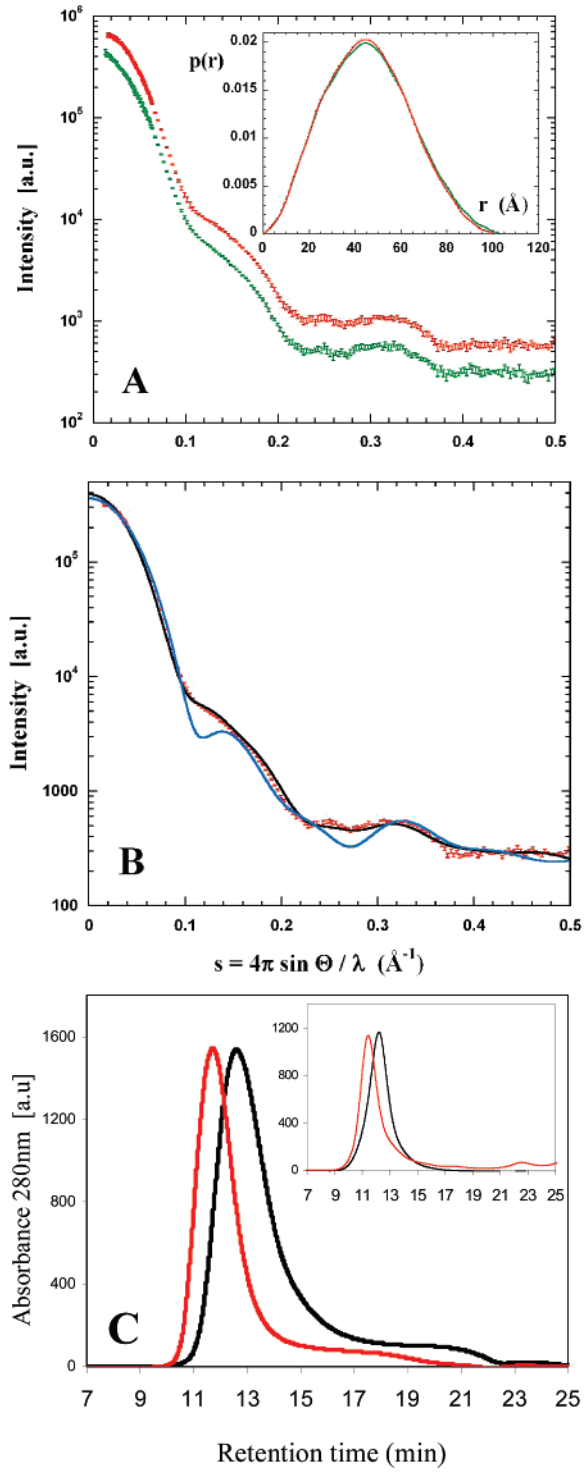

FIGURE 7: SAXS and simulated scattering profiles of the deletion mutant. Panel A: Experimental scattering profile of ligand-free (green) and 2′,5′-ADP-bound (red). For clarity the scattering profile of the 2′,5′-ADP-bound mutant has been artificially shifted upward by multiplying the intensity values (*y*-axis) by a factor of 2. Error bars for each scattering profile are shown. Inset: Intraparticle distance distribution function $p(r)$ for ligand-free (green line) and ligand-bound deletion mutant (red line). The areas under $p(r)$ are scaled to unity. Panel B: Reconstructed scattering profiles of the CPR-dimer models. NOS-based dimer model (blue line) and BUNCH model (black line). Panel C: Analytical gel filtration. Elution pattern of the wild-type CPR (black) and deletion mutant (red) (independent runs). The estimated molecular weight is ~70 kDa for wild-type enzyme and ~160 kDa for the deletion mutant. Inset: Elution pattern of two control proteins, albumin (66 kDa) and alcohol dehydrogenase (150 kDa). Axis units as in main panel C.

required for CPR's physiological function. Of particular interest is the contribution of these motions to the observed heat capacity change of the CPR−2′,5′-ADP interaction.

The concept of heat capacity has been central to the development of thermodynamics, and of physical sciences in general (*18*). Heat capacity is proportional to energy fluctuations in a system, and is a measure of the density of states accessible to that system; as such, it provides a microscopic interpretation of macroscopic thermodynamics (*19*). The theoretical basis for the contribution of conformational dynamics to the heat capacity change (ΔC_p) of protein−ligand interactions was laid out in a seminal work by Biltonen two decades ago (*20*). However, obtaining unequivocal experimental evidence for this has so far proved to be an intractable problem. This is largely due to the considerable difficulties involved in distinguishing the contribution of structural dynamics from other ligand-coupled state transitions which are normally major contributors to ΔC_p (i.e., coupled protonic equilibria; changes in solvation of the ligand and the protein binding site, and changes in the ligand conformation) (*20*). The approach employed here—targeting a functional loop located 60 Å away—constitutes a novel avenue to overcome these long-standing experimental problems.

To date, changes in heat capacity (ΔC_p) observed upon ligand binding to proteins have been explained in terms of discrete changes confined to the vicinity of the binding site (e.g., ligand hydrophobic surface burial, hydrogen-bond network disruption) (*21*, *22*). Heat capacity effects would then be dominated by ultrafast solvent and local vibrations (pico- and nanosecond time scale) (*23*). However, the results shown here demonstrate that the conformational constraints introduced by the poly-proline and deletion mutations at the interdomain loop affect not only enthalpy and entropy values associated to 2′,5′-ADP binding—in itself remarkable—but also the temperature dependence of those values, and hence, the heat capacity change (ΔC_p) values (Figure 2B, Table 1). The estimated ΔC_p values for these mutants are invariably more negative than for the wild-type enzyme, indicating a net reduction in available energy levels (*19*). This finding is consistent with our early observation that the ΔC_p for ligand binding to the isolated FAD-binding domain ($\Delta C_p = -300$ cal mol^{-1} K^{-1}) is significantly more negative than the value observed when the FAD-binding domain is linked to the FMN domain (i.e., 2′,5′-ADP binding within the entire CPR enzyme, $\Delta C_p = -220$ cal mol^{-1} K^{-1}) (Table 1) (*4*). Therefore the total density of states in this system must include a contribution from the microstates associated to the "other" domain (FMN-binding domain). The molecular envelopes of the 10P mutant (either ligand-free or the 2′,5′-ADP complex) show precisely a restriction of the spatial volume sampled by the structural domains in solution, as compared to the elongated arrangement adopted by the domains in the wild-type CPR (Figure 6). In the deletion mutant, with the most negative ΔC_p value (−580 cal mol^{-1} K^{-1}), dimerization would be conducive to a severe restriction in the rotational and translational degrees of freedom of the entire macromolecule. Interestingly, the SAXS data indicate that changes effected by ligand binding are indeed minimal in the deletion mutant (Figure 7A and inset, Table 2) (see Supporting Information). Additionally, the low rates observed with the deletion mutant suggest that, despite the close

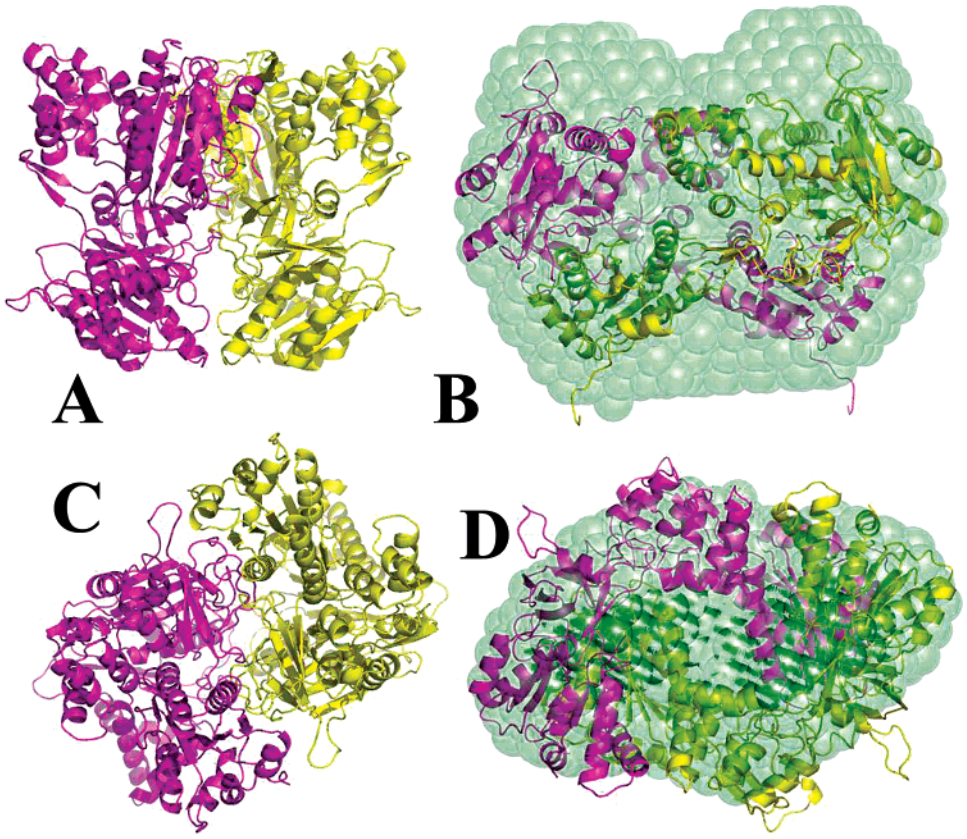

FIGURE 8: Dimer model of CPR and *ab initio* calculation of molecular envelope of the 2′,5′-ADP-bound deletion mutant. Panels A and C: Ribbon drawing of the CPR dimer model based on the dimer of the NOS CPR crystal structure (two perpendicular orientations with the monomers represented in purple and yellow colors). The simulated scattering profile of this NOS-based model is shown in Figure 7B. Panels B and D: Molecular shape of the dimer of 2′,5′-ADP-bound deletion mutant (green semitransparent spheres) restored from SAXS data with superimposed BUNCH model which provides a better fit to the experimental scattering data than the NOS-based model (Figure 7B). Two perpendicular views are presented in the same orientations as in A and C with both protomers highlighted in purple and yellow ribbons. The graphics were made with the program PYMOL (http://pymol.sourceforge.net).

packing, conformational sampling critically required for electron transfer has been severely limited in this mutant (Figures 3C and 4).

A rather puzzling feature of mutants' 2′,5′-ADP binding energetics is the additional heat released into the surroundings compared with the wild-type enzyme (Figure 2). The facts that the primordial interaction (2′,5′-ADP−R597) remains unchanged (Figure 3A) (Table 1) and the mutations take place 50−60 Å away rule out a modification of the ligand binding site as the cause of this enthalpy excess. Previous calorimetry studies have shown a similar enthalpy excess for 2′,5′-ADP binding to the isolated FAD-binding domain (i.e., in the absence of the FMN-binding domain). This amounts to $\sim$−4 kcal mol^{-1} at 35 °C, a 20% increase (see Figure 5A in ref *4*). Therefore, the conformational dynamics of the highly mobile FMN-binding domain appear to have a global effect in the observed energetics of 2′,5′-ADP binding (including ΔH_B). This conclusion is supported by the remarkable correlation between ligand binding's $T\Delta S_B$ values and turnover numbers for the reduction of cytochrome *c*, an event that requires motional shuttling of the FMN-binding domain (Figure 3C).

Isothermal titration calorimetry experiments are carried out at constant pressure and temperature in an open system. Under these (thermodynamic) constraints the evolution of the system to equilibrium corresponds to the extremization of Gibbs free energy, with entropy as the actual independent variable (enthalpy being the experimentally accessible conjugate variable). Extensive evidence from polymer science allows us to assert that the nature of the changes introduced upon these mutations are essentially entropic: insertion of poly-proline peptide reduces degrees of freedom by increasing the relative stiffness of the interdomain loop (Figure 3B) (*24*, *25*). This hindering effect appears to be even bigger in the deletion mutant as shown by calorimetry, kinetics, and SAXS data. This unfavorable entropic decrease would—*if uncompensated*—result in overall free energy being less favorable or even entirely nonspontaneous (i.e., positive ΔG_B). In classic thermodynamics theory, this is averted by the system releasing energy into the surroundings (the Second Law dictating that most of this energy must be released as heat, as opposed to work) (*26*). As a result, the system would be able to undergo this entropically unfavorable change while the total free energy change remains unaffected (isoergonic process) (*26*). We postulate this enthalpy exchange to be the origin of the heat excess observed in the mutants. It would then follow that the single protein macromolecule is actually displaying fundamental signatures of a real, independent ensemble, according to thermodynamics theory (*27*).

Early theoretical studies by Cooper (*28*, *29*) and Di Cera (*30*) put forward the notion that the (solvated) protein could be regarded as a formal ensemble, whose energetics would affect—and be affected by—events involving the entire macromolecule. An important corollary of this hypothesis

is the potential for transmission of structural information by way of fluctuations inherent to any real thermodynamic ensemble (*31*−*33*). Additionally, molecular dynamics studies on the microscopic origins of proteins' heat capacity by Karplus and co-workers postulated the existence of highly delocalized vibrational modes in the thermally accessible low-frequency regions, and highlighted these "slow" modes as ideal candidates for transfer information (i.e., binding energy transduction, conformational allostery) (*34*). Our observation that ligand binding can trigger global domain reorganization and that impairment of domain mobility (millisecond time scale) has an effect on the energetics of a distal ligand interaction (including its ΔC_p value) would agree indeed with these postulates. It would then appear that protein−ligand interactions do take place in an "extended interface", as suggested recently (*35*).

CONCLUSION

The combination of mutagenesis, calorimetry, kinetics, and *in solution X*-ray scattering reveals an interplay between the thermodynamics of ligand binding and domain conformational motion in human cytochrome P450 reductase. Remarkably, the energetics associated with 2′,5′-ADP binding appear to report on the entire multidomain protein. These results provide a conceptual framework for understanding similar long-range structural effects (involving coenzyme binding) observed in other members of this important protein family, such as nitric-oxide synthase (*37*−*41*). The deletion mutant would then constitute an intermediate model between CPR (monomer) and neuronal NOS (dimer). Crystallography studies of this mutant are now in progress.

ACKNOWLEDGMENT

We would like to thank John E. Ladbury (UCL, London) for helpful discussions and constant encouragement during this work. We are very grateful to Gordon C. K. Roberts (University of Leicester) for sharing his allocated beam-time at Daresbury Synchrotron Source (U.K.). We are indebted to Alan Cooper and Margaret Nutley (University of Glasgow) for insightful comments and technical assistance with DSC experiments, and to Wei-Cheng Huang (University of Leicester) for skillful help with HPLC analytical gel filtration.

SUPPORTING INFORMATION AVAILABLE

Thermal unfolding (DSC) of wild-type CPR, 10P, and deletion mutant. *Ab initio* shape reconstruction of the deletion mutant in the presence and absence of 2′,5′-ADP. This material is available free of charge via the Internet at http://pubs.acs.org.

REFERENCES

1. Wang, M., Roberts, D. L., Paschke, R., Shea, T. M., Masters, B. S., and Kim, J. J. (1997) Three-dimensional structure of NADPH-cytochrome P450 reductase: prototype for FMN- and FAD-containing enzymes, *Proc. Natl. Acad. Sci. U.S.A. 94*, 8411−8416.
2. Gutierrez, A., Lian, L-Y., Wolf, C. R., Scrutton, N. S., and Roberts, G. C. (2001) Stopped-flow kinetic studies of flavin reduction in human cytochrome P450 reductase and its component domains, *Biochemistry 40*, 1964−1975.
3. Gutierrez, A., Paine, M., Wolf, C. R., Scrutton, N. S., and Roberts, G. C. (2002) Relaxation kinetics of cytochrome P450 reductase: internal electron transfer is limited by conformational change and regulated by coenzyme binding, *Biochemistry 41*, 4626−4637.
4. Grunau, A., Paine, M. J., Ladbury, J. E., and Gutierrez, A. (2006) Global effects of the energetics of coenzyme binding: NADPH controls the protein interaction properties of human cytochrome P450 reductase, *Biochemistry 45*, 1421−1434.
5. Fisher, H. F., and Singh, N. (1995) Calorimetric methods for interpreting protein- ligands interactions, *Methods Enzymology 259*, 194−221.
6. Cooper, M. A., and Wadood, N. A. (2000) Differential scanning microcalorimetry, in *Protein-ligand interactions hydrodynamics and calorimetry* (Harding, S. E., and Chowdhry, B. Z, Eds.) Oxford University Press, Oxford, New York.
7. Grossmann, J. G., Crawley, J. B., Strange, R. W., Patel, K. J., Murphy, L. M., Neu, M., Evans, R. W., and Hasnain, S. S. (1998) The nature of ligand-induced conformational change in transferin in solution. An investigation using X-ray scattering, XAFS and site-directed muatagenesis, *J. Mol. Biol. 279*, 461−472.
8. Svergun, D. I. (1992) Determination of the regularization parameter in indirect-transform methods using perceptual criteria, *J. Appl. Crystallogr. 25*, 495−503.
9. Svergun, D. I., Petoukhov, M. V., and Koch, M. H. J. (2001) Determination of domain structure of proteins from X-ray solution scattering, *Biophys. J. 80*, 2947−2953.
10. Volkov, V. V., and Svergun, D. L. (2003) Uniqueness of ab initio shape determination in small angle scattering, *J. Appl. Crystallogr. 36*, 860−864.
11. Kneller, D. G., Cohen, F. E., and Langredge, R. (2001) Automated matching of high- and low-resolution strucutural models, *J. Appl. Crystallogr. 34*, 33−41.
12. Garcin, E. D., Bruns, C. M., Lloyd, S. J., Hosfield, D. J., Tiso, M., Gachhui, R., Stuehr, D. J., Tainer, J. A., and Getzoff, E. D. (2004) Structural basis for isozyme-specific regulation of electron transfer in nitric-oxide synthase, *J. Biol. Chem. 279*, 37918−37927.
13. Svergun, D., Barberato, C., and Koch, M. H. J. (1995) *CRYSOL*—a program to evaluate X-ray solution scattering of biological macromolecules from atomic coordinates, *J. Appl. Crystallogr. 28*, 768−773.
14. Zhang, J., Martasek, P., Paschke, R., Shea, T., Masters, B. S. S., and Kim, J-J. P. (2001) Crystal Structure of the FAD/NADH-binding domain of rat neuronal nitric-oxide synthase, *J. Biol. Chem. 276*, 37506−37513.
15. Neeli, R., Girvan, H. M., Lawrence, A., Warren, J. W., Leys, D., Scrutton, N. S., and Munro, A. W. (2005) The dimeric form of flavocytochrome P450 BM3 is catalytically functional as a fatty acid hydrxylase, *FEBS Lett. 579*, 5582−5588.
16. Page, C. C., Moser, C. C., and Dutton, P. L. (2003) Mechanism for electron transfer within and between proteins, *Curr. Opin. Chem. Biol. 7*, 551−556.
17. Gutierrez, A., Munro, A. W., Wolf, C. R., Scrutton, N. S., and Roberts, G. C. K. (2003) Interflavin electron transfer in human cytochrome P450 reductase is enhanced by coenzyme binding : relaxation kinetics studies with coenzyme analogues, *Eur. J. Biochem. 270*, 2612−262.
18. Rogers, D. W. (2005) *The Plank-Bose-Einstein Theory of Heat Capacity*, Princeton University Press, Princeton, NJ.
19. Prabhu, N. V., and Sharp, K. A. (2005) Heat capacity in proteins, *Annu. Rev. Phys. Chem. 56*, 521−548.
20. Eftink, M. R., Anusiem, A. C., and Biltonen, R. L. (1983) Enthalpy-entropy compensation and heat capacity changes for protein-ligand interactions: General thermodynamic model and data for the binding of nucleotides to ribonuclease A, *Biochemistry 22*, 3884−3896.
21. Loladze, W., Ermolenko, D. N., and Makhatadze, G. I. (2001) Heat Capacity changes upon burial of polar and nonpolar groups in proteins, *Protein Sci. 10*, 1343−1352.
22. Bergqvist, S., Williams, M. A., O'Brien, R., and Ladbury, J. E. (2004) Heat capacity effects of water molecules and ions at a protein-DNA interface, *J. Mol. Biol. 336*, 829−842.
23. Lee, A. L., and Wand, J. (2001) Microscopic origins of entropy, heat capacity and the glass transition in proteins, *Nature 411*, 501−504.
24. Sun, S. F. (2004) *Physical Chemistry of Macromolecules*, 2nd ed., Wiley & Sons, NJ.
25. Schimmel, P. R., and Flory, P. J. (1967) Conformational energy and configurational statistics of poly-L-proline, *Proc. Natl. Acad. Sci. U.S.A. 57*, 52−59.

26. Landau, L. D., and Lifshitz, E. M. (1980) *Statistical Physics* (Course of Theoretical Physics Vol. 5, Part 1, 3rd ed.) Elsevier, Oxford.
27. Hallerbach, B., and Hinz, H-J. (2000) Protein heat capacity reflects the dynamics of enthalpy exchange between the single macromolecule and the surroundings, *Proteins: Struct., Funct., Genet. 4*, 86−92.
28. Cooper, A. (1976) Thermodynamic fluctuations in protein molecules, *Proc. Natl Acad. Sci. U.S.A. 73*, 2740−2741.
29. Cooper, A. (1984) Protein fluctuations and the thermodynamic uncertainty principle, *Prog. Biophys. Mol. Biol. 44*, 181−214.
30. Di Cera, E. (1995) *Thermodynamic Theory of Site-Specific Binding Processes in Biological Macromolecules*, Cambridge University Press, Cambridge.
31. Cooper, A., Dryden, D. T. F. (1984) Allostery Without Conformation Change, *Eur. Biophys. J. 11*, 103−109.
32. Milev, S., Bjelic, S., Georgiev, O., and Jelesarov, I. (2007) Energetics of peptide recognition by the second PDZ domain of human protein tyrosine phosphatase 1E, *Biochemistry 46*, 1064−1078.
33. Hilser, V. J., Dowdy, D., Oas, T. G., and Freire, E. (1998) The structural distribution of cooperative interactions in proteins: Analysis of the native state ensemble, *Proc. Natl. Acad. Sci. U.S.A. 95*, 9903−9908.
34. Brooks, B., and Karplus, M. (1983) Harmonic dynamics of proteins: normal modes and fluctuations in bovine pancreatic inhibitor, *Proc. Natl. Acad. Sci. U.S.A. 80*, 6571−6575.
35. Ladbury, J. E., and Williams, M. A. (2004) The extended interface: measuring non-local effects in biomolecular interactions, *Curr. Opin. Struct. Biol. 14*, 562−569.
36. Petoukhov, M. V., and Svergun, D. I. (2005). Global rigid body modelling of macromolecular complexes against small-angle scattering data, *Biophys. J. 89*, 1237- 1250.
37. Craig, H. D., Chapman, S. K., and Daff. S. (2002) Calmodulin activates electron transfer through neuronal nitric-oxide synthase reductase domain by releasing an NADPH-dependent conformational lock, *J. Biol. Chem. 277*, 33987−33994.
38. Knudsen, G. M., Nishida, C. R., Mooney, S. D., and Ortiz de Montellanos, P. R. (2003) Nitric-oxice synthase (NOS) reductase domain models suggest a new control element in endothelial NOS that attenuates calmodulin-dependent activity, *J. Biol. Chem. 278*, 31814−31824.
39. Tiso, M., Konas, D. W., Panda, K., Garcin, E. D., Sharma, M, Getzoff, E. D., and Stuehr, D. J. (2005) C-terminal tail redidue Arg^{1400} enables NADPH to regulate electron transfer in neuronal nitric-oxide synthase, *J. Biol. Chem. 280*, 39280−39219.
40. Roman, L. J., and Masters, B. S. (2006) Electron transfer by neuronal nitric-oxide synthase is regulated by concerted interaction of calmodulin and two intrinsic regulatory elements, *J. Biol. Chem. 281*, 23111−23118.
41. Dunford, A. J., Rigby, S. E. J., Hay, S., Munro, A. W., and Scrutton, N. S. (2007) Conformational and thermodynamic control of electron transfer in neuronal nitric oxide synthase, *Biochemistry 46*, 5018−5029.
42. Konarev, P. V., Petoukhov, M. V., Volkov, V. V., and Svergun, D. I. (2006) ATSAS 2.1, a program package for small-angle scattering data analysis, *J. Appl. Crystallogr. 39*, 277−286.

BI700596S